

DNA Damage Response and Inflammatory Signaling Limit the MLL-ENL-Induced Leukemogenesis In Vivo

Sylvia Takacova,¹ Robert Slany,⁴ Jirina Bartkova,⁵ Viktor Stranecky,⁶ Petr Dolezel,¹ Pavla Luzna,^{1,2} Jiri Bartek,^{3,5,*} and Vladimir Divoky^{1,*}

¹Department of Biology

²Department of Histology and Embryology

³Institute of Molecular and Translational Medicine

Faculty of Medicine and Dentistry, Palacky University, 77515 Olomouc, Czech Republic

⁴Department of Genetics, University Erlangen, D-91058 Erlangen, Germany

⁵Danish Cancer Society Research Center, DK-2100 Copenhagen, Denmark

⁶Institute of Inherited Metabolic Disorders, Charles University in Prague, First Faculty of Medicine, 12808 Prague, Czech Republic

*Correspondence: jb@cancer.dk (J.B.), divoky@tunw.upol.cz (V.D.)

DOI 10.1016/j.ccr.2012.01.021

SUMMARY

Activation of the MLL-ENL-ERtm oncogene initiates aberrant proliferation of myeloid progenitors. Here, we show induction of a fail-safe mechanism mediated by the DNA damage response (DDR) machinery that results in activation of the ATR/ATM-Chk1/Chk2-p53/p21^{CIP1} checkpoint and cellular senescence at early stages of cellular transformation caused by a regulatable MLL-ENL-ERtm in mice. Furthermore, we identified the transcription program underlying this intrinsic anticancer barrier, and DDR-induced inflammatory regulators that fine-tune the signaling toward senescence, thereby modulating the fate of MLL-ENL-immortalized cells in a tissue-environment-dependent manner. Our results indicate that DDR is a rate-limiting event for acquisition of stem cell-like properties in MLL-ENL-ERtm-mediated transformation, as experimental inhibition of the barrier accelerated the transition to immature cell states and acute leukemia development.

INTRODUCTION

During the multistep pathogenesis of leukemia, a pool of leukemia stem cells (LSCs) emerges, capable of limitless self-renewal and disease maintenance. LSCs can originate from hematopoietic cells at different developmental stages. Mixed-lineage leukemia (MLL) fusion oncogenes can transform committed progenitors to LSCs by reactivation of a self-renewal-associated transcription program (Cozzio et al., 2003; Krivtsov et al., 2006). Several mouse models showed that *Mll* fusions expressed at physiological levels cause myeloproliferation without the capacity to propagate the disease in transplanted animals (Dobson et al., 1999; Wang et al., 2005). *Mll* fusions initiate the preleukemia stem cell (pre-LSC) state, and

acquisition of further mutations or high dosage of oncogene expression is necessary for full transformation and development of acute leukemia (Wang et al., 2005; Chen et al., 2008).

Research on solid tumors has identified a DDR barrier at early pre-invasive stages of tumorigenesis. Oncogene-induced hyperproliferation and DNA replication stress trigger the cell-intrinsic DDR machinery that induces senescence or cell death and delays progression to full malignancy (Bartkova et al., 2005, 2006; Gorgoulis et al., 2005; Di Micco et al., 2006; Halazonetis et al., 2008). Recent studies have suggested that DDR cooperates with secreted cytokines in balancing the signaling thresholds and cell-fate decisions between cell proliferation, senescence and death (Bartek et al., 2008; Rodier et al., 2009; Acosta et al., 2008). However, an authentic model to assess

Significance

DNA damage response (DDR) signaling and senescence may pose a biological barrier to progression of diverse types of solid tumors, in part by an ill-defined interplay with inflammatory cytokines. Demonstrating the existence, and understanding the role of analogous phenomena in leukemia may provide novel insights into the molecular pathogenesis and biological complexity of hematological malignancies. Using a mouse model with long latency of mixed-lineage leukemia (MLL) development, we identify DDR as a critical mechanism rate-limiting for malignant transformation by the MLL-ENL oncogene, synergizing with inflammatory factors in checkpoint signaling and senescence, thereby counteracting leukemogenesis. This in vivo model of DDR and inflammatory barriers cooperating in their natural settings has implications for understanding cancer stem cell evolution and multistep tumorigenesis.

such candidate DDR and cytokine barriers during the long-latency development of any malignancy *in vivo* is still missing.

Inspired by these recent developments, we wished to examine whether a DDR- and/or cytokine-related barrier analogous to solid tumors and oncogene-transformed fibroblasts might also impact leukemogenesis. In addition, we wished to test the potential significance of the barrier concept in an adequate animal model. To address these issues, we generated a conditional mouse model, in which the *Mll-ENL* fusion oncogene is expressed in the physiological context of the endogenous *Mll* locus and its activity is regulatable with tamoxifen *in vivo*.

RESULTS

Generation of a Regulatable *Mll-ENL-ERtm* Knock-In Mouse

We created a mouse model wherein the protein function of the *Mll-ENL* oncogene depends on tamoxifen (TAM) or 4-hydroxytamoxifen (4-oht) due to fusion with the mutated estrogen-binding domain of the estrogen receptor (ERtm) (Littlewood et al., 1995). The *Mll-ENL-ERtm* fusion gene was used to engineer the mouse knock-in allele in the v6.5 mouse embryonic stem cells (ESCs) (Figure 1A; Figures S1A and S1B available online). We confirmed the expression of the *Mll-ENL-ERtm* allele in c-Kit⁺ hematopoietic progenitors isolated from the BM of the knock-in mice (Figure S1C). The transcriptional transactivation activity of the fusion gene and serial replating ability of the *Mll-ENL-ERtm* c-Kit⁺ BM cells were strictly dependent on 4-oht (Figures S1D and S1E).

Activated *MLL-ENL-ERtm* Induces Myeloproliferation in Both BM and Spleen with Different Hematopoietic Characteristics

After 7 months of TAM administration, the *Mll-ENL-ERtm* mice developed a myeloproliferative disease with a 100% penetrance, which progressed into the terminal stage in five of ten animals after a long period (mean survival: 592 ± 112 days) of continuous TAM provision. To study early and late phenotypic characteristics of the *MLL-ENL-ERtm*-mediated disease *in vivo*, we monitored hematopoiesis in the *Mll-ENL-ERtm*/TAM mice at the early (7 months) and terminal stage of disease. Time-matched TAM-treated wild-type mice served as controls for both stages. Early changes in the BM were characterized by hypercellularity with expansion of mature myeloid elements (band neutrophils) (Figures 1B and S2A), consistent with fluorescence-activated cell sorting (FACS) analysis showing an increase in Mac-1⁺/Gr-1⁺ cell population and emergence of a c-Kit⁺/Mac-1⁺ subpopulation in some animals (Figure 1C). At this time point, a left shift in granulopoiesis occurred with an increase of band neutrophils and monocytes at the expense of lymphocytes in the spleen (Figure S2B). The myeloid expansion in the spleen progressed at the terminal stage of disease (Figure 1D, right). This was associated with a gradual increase of Mac-1⁺/Gr-1⁺ myeloid cells and a decrease of B220⁺/CD19⁺ and CD19⁺/IgM⁺ B-lymphoid cells. Notably, there was an expansion of the c-Kit⁺/Mac-1⁺ subpopulation (Figure 1E). The terminal stage was also associated with high numbers of white blood cells, large numbers of mature segmented neutrophils, less mature band neutrophils and only a few percent of myeloblasts in the peripheral blood. There was occasionally a left shift in granulopoiesis and elevated monocytes (Figure 1F), and myeloid infiltration into the liver and kidney (Figure S2C). Some mice developed solid tumors in the mesenterium, formed by *Mll-ENL-ERtm* positive myeloid cells (data not shown), indicating the invasive and angiogenic nature of the *MLL-ENL-ERtm*-transformed cells. The initial expansion of the granulocytic lineage in the BM eventually culminated in a virtual depletion of the tissue over time. Thus, activation of the *MLL-ENL-ERtm* oncogene leads to abnormal expansion of the granulocytic lineage in the BM and granulo-monocytic lineages in the spleen with a potential to progress into a malignant phenotype.

Mll-ENL-ERtm hematopoietic progenitors derived from both tissues at the early stage showed increased 4-oht-dependent myeloid colony forming ability in methylcellulose cultures. In the absence of 4-oht, both CFU-GM and CFU-G colonies were lower in numbers, size, and cellularity (Figures 2A and 2B, top and bottom right panels). Besides the typical CFU-GM and CFU-G colonies, we often found colonies that were hypercellular and appeared more immature (Figure 2B, top left panel). These results suggest that the active *MLL-ENL-ERtm* oncogene enhances proliferation and increases survival of committed myeloid progenitors, features that could be reverted after deactivation of the oncogene. Colonies did not grow in the absence of growth factors and cytokines (with or without 4-oht) suggesting that *MLL-ENL-ERtm* does not confer growth factor-independent properties to immortalized progenitors.

MLL-ENL-ERtm hematopoietic progenitors derived from both tissues at the early stage showed increased 4-oht-dependent myeloid colony forming ability in methylcellulose cultures. In the absence of 4-oht, both CFU-GM and CFU-G colonies were lower in numbers, size, and cellularity (Figures 2A and 2B, top and bottom right panels). Besides the typical CFU-GM and CFU-G colonies, we often found colonies that were hypercellular and appeared more immature (Figure 2B, top left panel). These results suggest that the active *MLL-ENL-ERtm* oncogene enhances proliferation and increases survival of committed myeloid progenitors, features that could be reverted after deactivation of the oncogene. Colonies did not grow in the absence of growth factors and cytokines (with or without 4-oht) suggesting that *MLL-ENL-ERtm* does not confer growth factor-independent properties to immortalized progenitors.

MLL-ENL-ERtm-Induced Proliferation/Self-Renewal of Myeloid Cells Leads to Activation of a Fail-Safe Mechanism

Given the observed distinct patterns of disease in the two tissues, we next examined the proliferation rates of the expanded Mac-1⁺ cell population in the BM and spleen of the *Mll-ENL-ERtm*/TAM mice by estimating bromodeoxyuridine (BrdU) incorporation at four time points: 7, 8, 9, and 10 months. There was a striking difference in cell proliferation between the two sites. The vast majority (90%) of Mac-1⁺ cells in the BM showed BrdU-positivity at 7 months of TAM treatment, followed by a dramatic loss of their long-term proliferative potential, as evidenced at the 8-month time point by the lack (below 1%) of BrdU incorporation. In contrast, the initial hyperproliferation of Mac-1⁺ cells was more moderate in the spleen (40.4% of BrdU⁺ at 7 months) and importantly, proliferating Mac-1⁺ cells were reduced yet remained clearly detectable also during disease progression at the 9- and 10-month time points (23.8% BrdU⁺ among Mac-1⁺ cells) (Figures 3A, 3C, left, and 3E).

These findings prompted us to test whether the proliferation phenotypes could reflect induction of a fail-safe mechanism, possibly differentially in the BM versus spleen. To address this question, we examined total BM cells and spleen sections (from the *Mll-ENL-ERtm*/TAM mice that were used for the BrdU-incorporation assay) for the senescence-associated beta-galactosidase (SA-β-gal) (Dimri et al., 1995). In the BM, SA-β-gal was induced in neutrophils (Figure 3B) in parallel with the loss of their proliferative potential by 8 months of TAM treatment (Figure 3E, left). Consistent with reduced proliferation of Mac-1⁺ cells in the spleen, we detected an accumulation of SA-β-gal above the physiological level in the *Mll-ENL-ERtm*/TAM mice (9–10 months of TAM) compared to wild-type/TAM

controls (Figure 3C, right). Compared to early stage (7 months of TAM treatment), spleen displayed decreased proliferation and appearance of SA- β -gal⁺ cells at the 9- to 10-month time points (Figures 3C and 3E, right). These results suggest a balanced state of proliferation and senescence in the expanding myeloid cell population in the spleen. Collectively, these findings indicate that the MLL-ENL-ERtm-initiated hyperproliferation is followed by induction of cellular senescence that counteracts the aberrant proliferation of Mac-1⁺ cells, a process that is more robust in the BM compared with the spleen.

The ATR-Chk1 DDR Pathway Is Activated in the Mac-1⁺ Population

The MLL-ENL-ERtm-induced hyperproliferation and senescence prompted us to search for potential activation of DNA damage signaling, a response to oncogene-evoked replication stress reported for human cells and solid tumors (Halazonetis et al., 2008). Indeed, phosphorylation of the ataxia telangiectasia mutated and RAD3-related kinase at serine 428 (pATRS428), which is induced in response to replication-associated DNA damage, was detected in the majority of Mac-1⁺ cells both in the BM and spleen, coincident with the early MLL-ENL-ERtm-induced hyperproliferation (7 months of TAM treatment), in contrast to absence of pATRS428 in Mac-1⁺ cells of either organ in wild-type/TAM control mice (Figure S3A). Importantly, data very similar to pATRS428 were obtained by both immunohistochemistry and immunofluorescence using a recently published antibody against ATR autophosphorylated at threonine 1989 (T1989) (Figures 3D and S3A), a site crucial for ATR activation (Liu et al., 2011; Nam et al., 2011). The specificity of the two antibodies to phosphorylated ATR was validated using a number of tests and models including ATR-deficient control cells (Figure S3B; and data not shown). Given the consistent results seen with both antibodies, we refer to both markers collectively as pATR. Consistently, pATR was accompanied by downstream markers of ATR signaling, including histone H2AX phosphorylated at serine 139 (γ H2AX) and checkpoint kinase 1 (Chk1) phosphorylated at serine 345 (pChk1S345) in Mac-1⁺ cells in both BM and spleen (Figure 3D).

To examine whether DDR signaling persists across disease stages, we followed the level of pATR and the γ H2AX signal at the time points assessed for proliferation and senescence. Analogous to proliferation and senescence phenotypes, there was a striking difference in the ATR-linked signaling between BM and spleen. In the BM, there was an increase both in the nuclear γ H2AX signal intensity (data not shown) and number of Mac-1⁺/ γ H2AX⁺ cells that correlated inversely with the number of Mac-1⁺/BrdU⁺ cells in the transition period to senescence between 7 and 8 months of TAM treatment (Figure 3E, left). Interestingly, pATR became undetectable and the intensity of γ H2AX was decreased (but not eliminated) in the senescent cells (Figure S3C). In contrast to BM, pATR was present both during the early (proliferative) and progression stages concomitant even with the partial senescence phenotype in the spleen (Figure S3D), a scenario that is consistent with partly ongoing proliferation and less pronounced γ H2AX compared to BM (Figure 3E, right).

Collectively, these results indicate that in response to MLL-ENL, DDR is indeed activated *in vivo*, and to a higher degree in BM compared to spleen. Increased signaling of the ATR pathway

and decrease in proliferation are gradual processes that precede senescence in the BM. The extent of DDR signaling correlates well with the efficiency of senescence induction in BM versus spleen, suggesting the signaling threshold may be influenced by the local tissue microenvironment.

ATM Is Required for an Effective Activation of the p53/p21^{CIP1} Pathway

The differences in γ H2AX patterns between BM and spleen, and partial persistence of γ H2AX in the BM even after loss of pATR led us to test whether the ataxia telangiectasia-mutated (ATM) kinase might be activated in response to MLL-ENL, particularly in the BM. Indeed, the early proliferation disease stage in the BM was associated with moderate levels of activated ATM phosphorylated at serine 1981 (pATMS1981 and pATM) seen as one to two nuclear foci in about 12% of cells. The level of pATM gradually increased to 43% of cells, and five to ten foci in most nuclei, during the transition toward senescence (Figures 4A, top, and 4B). Furthermore, active p53 (phosphorylated at serine 18, p-p53Ser18) and enhanced expression of its transcriptional target *p21^{CIP1}* (Figures 4A, bottom, and 4C) became apparent, in parallel with high levels of pATM. pATM was detectable in ~90% of myeloid cells in the senescent state of the MLL-ENL-ERtm/TAM BM (Figure 4D) consistent with the high proportion of γ H2AX⁺/Mac-1⁺ cells. Notably, ATM was not activated in the spleen (data not shown), consistent with the overall lower extent, and gradual elimination of DDR in this tissue. In contrast to the activated DDR signaling, we did not detect any increase of *p16^{INK4A}* mRNA or protein expression in the senescent BM (data not shown).

These results indicate that gradually increasing MLL-ENL-induced DDR, through combined ATR and ATM signaling, may lead to preferential activation of p53/p21^{CIP1} and more robust proliferation arrest and cellular senescence in the BM, compared to overall milder phenotypes and lack of ATM activation in the spleen.

Gene Expression Signatures of the Transition from Proliferation to Senescence

To better understand the MLL-ENL-induced dynamic cellular phenotypes and identify potential regulators of the observed cell states, we next profiled gene expression at three time points: 1), the early high proliferation with low DDR signaling; 2), the transition period of lower proliferation and high DDR activity; and 3), the senescence in the BM. Compared to BM from matched wild-type/TAM controls at each time point, gene ontology (GO) annotations of upregulated transcripts revealed enrichment of genes related to innate and adaptive immune response across the entire time course analyzed (Figure 5A). Using a pairwise analysis, we then determined unique and shared expression patterns among the three time points (Figure 5B). The shared immune response genes included those implicated in cell migration and localization, such as *Cx3cr1*, *Ccr1*, *Ccl9*, and *Vav3*, leukocyte activation, such as *Nfam1* or *Slc11a1*, and G protein coupled receptor pathways (*Emr1*, *Emr4*). Furthermore, toll-like receptor (*Tlr*) genes, implicated in cancer and in innate and adaptive immune responses through activation of cytokine and chemokine production (Rakoff-Nahoum and Medzhitov, 2009), were upregulated uniquely in the early proliferation (*Tlr5*), or

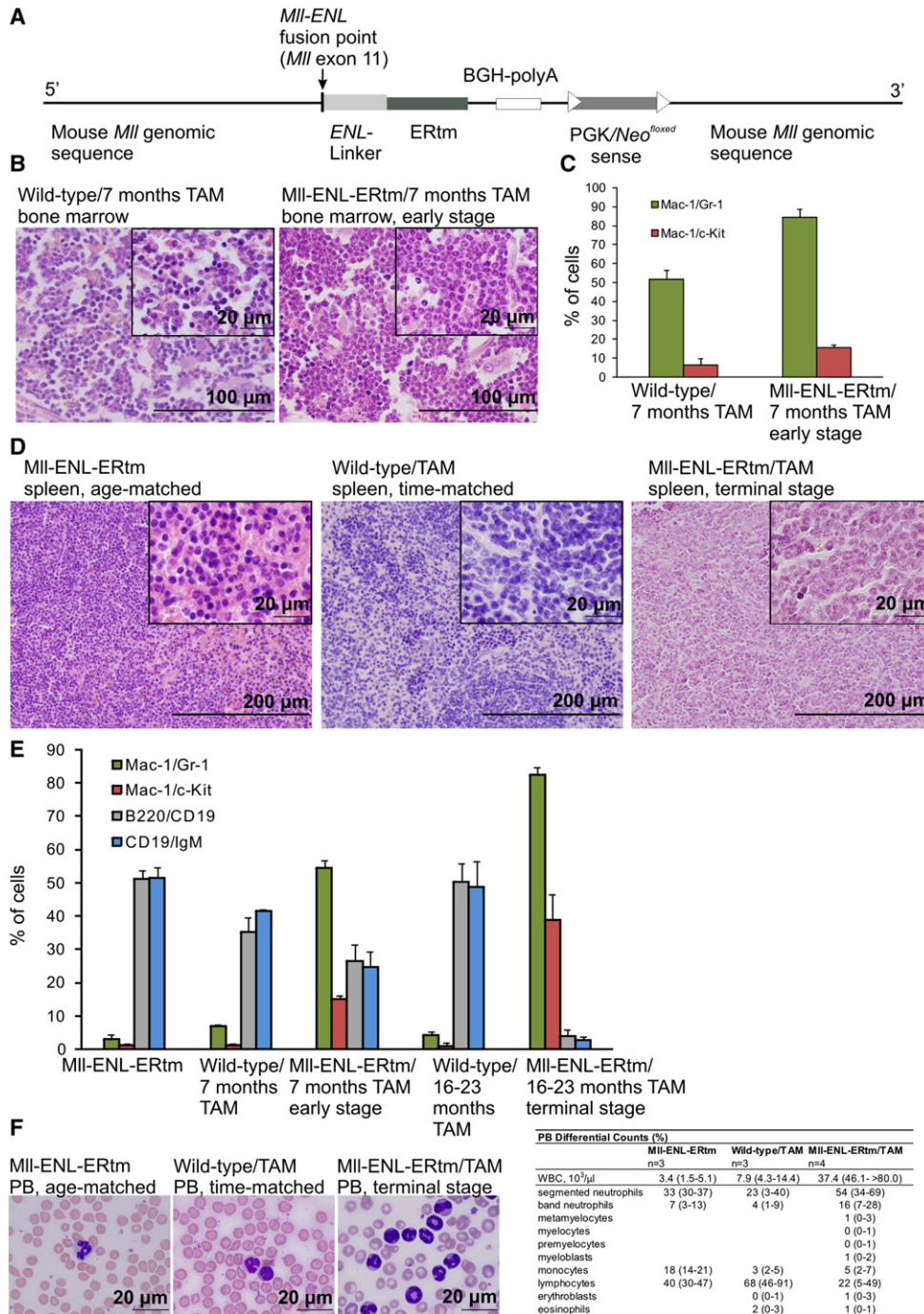


Figure 1. Myeloproliferation in the MII-ENL-ERtm Mice

(A) Schematic representation of the *MII-ENL-ERtm/Neo^{floxexd}* knock-in allele. The *MII-ENL* fusion point, the estrogen receptor binding domain (ERtm), polyadenylation site (BGH-polyA), and neomycin resistance gene under the phosphoglycerate kinase promoter (PGK/*Neo^{floxexd}*) are shown.

(B) Histopathology images: hypercellularity and expansion of mature myeloid cells in the BM of the MII-ENL-ERtm mice at the early stage of disease compared to wild-type/TAM control. Scale bars represent 100 μm and 20 μm (inset).

(C) FACS determined an increase in Mac-1⁺/Gr-1⁺ and Mac-1⁺/c-Kit⁺ cells in the BM of early disease stage MII-ENL-ERtm/TAM mice compared to wild-type/TAM animals. Data represent average cell percentages counted from three mice ± SD.

(D) Spleen histology, expansion of extramedullary hematopoiesis and disruption of the splenic architecture at the terminal stage of disease (right). Scale bars represent 200 μm and 20 μm (inset).

(E) Time course of indicated marker expression at 7 and 16–23 months of TAM treatment in the spleen of the MII-ENL-ERtm/TAM mice compared to wild-type/TAM mice shows expansion of Mac-1⁺/Gr-1⁺ and Mac-1⁺/c-Kit⁺ myeloid cells, and decrease in B220⁺CD19⁺, CD19⁺IgM⁺ B lymphoid cells. Data represent average cell percentages measured by FACS, counted from three mice ± SD.

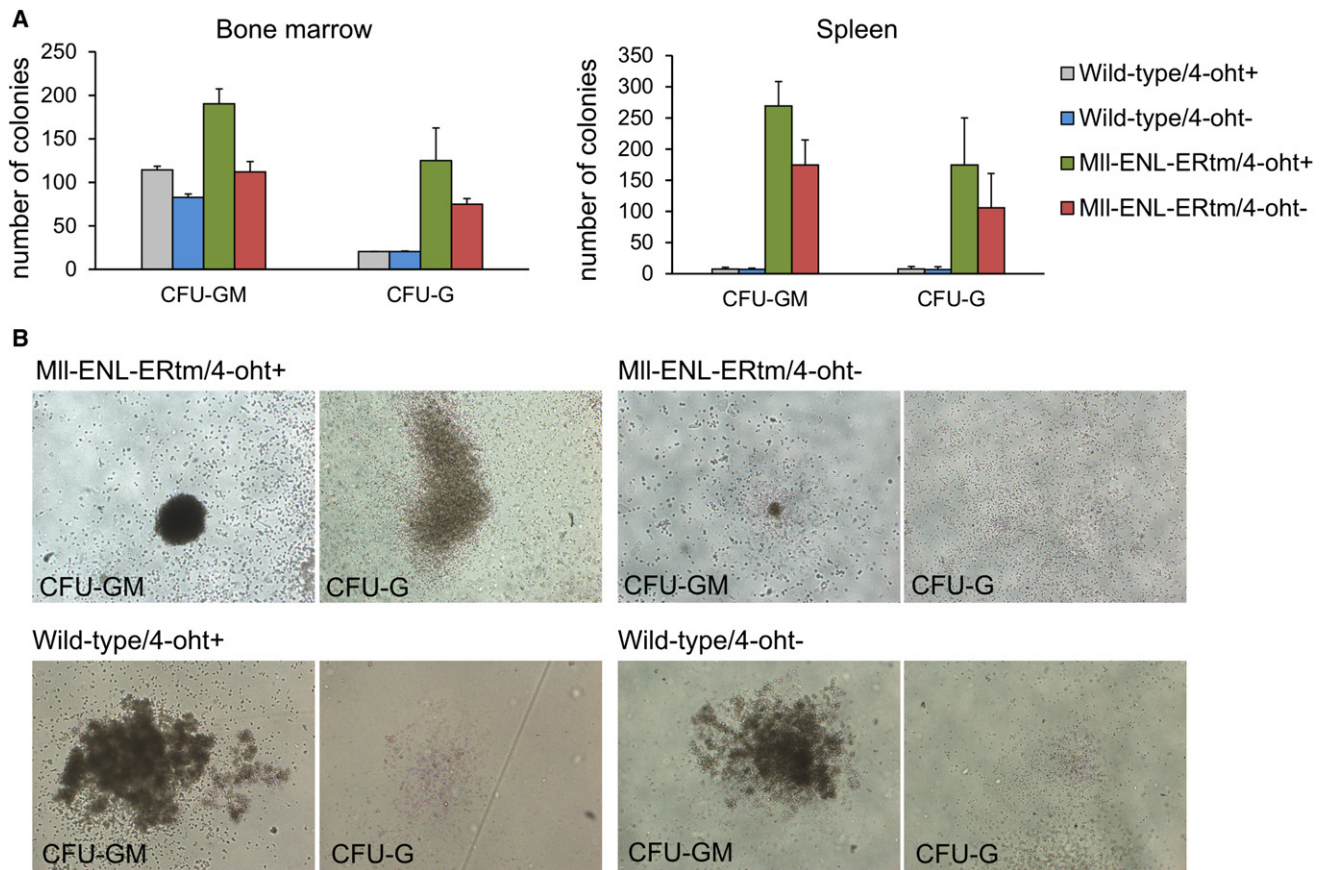


Figure 2. MLL-ENL-ERtm-Dependent Proliferation and Survival of Committed Myeloid Progenitors

(A) Increased myeloid colony formation of the MII-ENL-ERtm BM (left) and spleen (right) cells derived from TAM-treated mice at early disease stage compared to wild-type/TAM controls. Note lower colony numbers in the absence of 4-oht (experiments performed in duplicates, data represent average colony numbers from two mice \pm SD). The same color coding was used for both graphs.

(B) MII-ENL-ERtm CFU-GM and CFU-G colonies show an immature phenotype in the presence of 4-oht: CFU-GM colonies with compact centers without the halo of single cells and hypercellular, dense CFU-G colonies (top left). Note reversion of the immortalized phenotype and loss of colony formation capacity of the MII-ENL-ERtm CFU-GMs and CFU-Gs in the absence of 4-oht (top right).

See also Figure S2.

during both the proliferation and transition periods (*Tlr6*). Downstream mediators of TLR signaling, such as *Tnfsf14* (linked to NF- κ B signaling), and MAPK and JNK kinase pathway genes such as *Map3k5* and *Fgd4*, were upregulated in the proliferation state. A set of inflammatory response genes such as *Il1f9*, *Nfkbiz*, *Stat6*, *Il1rn*, and *Tnfrsf1b* were upregulated during the proliferation and transition states, and so were two pattern recognition receptors, *Clec7a* and *Clec2i*, implicated in cytokine production.

Another set of genes was strongly yet transiently upregulated only during the transition period of high DDR signaling, followed by a drop to basal levels in senescence. These included immediate early genes such as *Jun*, *Junb*, *Egr1*, *Egr2*, *Zfp36*, *Ier2* and *Ier3*, and *Cebpb*, a candidate key regulator of inflammatory cytokine and chemokine production in oncogene-induced

senescence (Acosta et al., 2008). Regulators of inflammation, including chemokine genes *Cxcl2*, *Ccl3*, and *Ccl4*, two key cytokine genes *Tnfa* and *Il1b*, and *Ptgs2*, associated with tumor-promoting inflammation (Wang and Dubois, 2010), were also upregulated (Figure 5C).

For the spleen, differential gene expression profiles were determined for three stages: 1), early (proliferation, induced DDR); 2), progression (partial senescence, DDR maintained); and 3) terminal (proliferation, low or absent DDR, no senescence). By pairwise analysis, we found a set of genes differentially expressed at the early stage and maintained their pattern during disease progression. The upregulated genes were enriched in cell cycle regulators. Interestingly, downregulated genes were enriched in innate immunity genes, acute phase

(F) Representative PB smear with abundant mature myeloid cells (scale bar represents 20 μ m) and PB differential counts with a left shift in granulopoiesis at the terminal disease stage. Data are average (data range) from three to four mice, respectively. Data from untreated MII-ENL-ERtm mice age-matched to leukemic mice at the terminal disease stage are also shown in (D-F).

See also Figure S1.

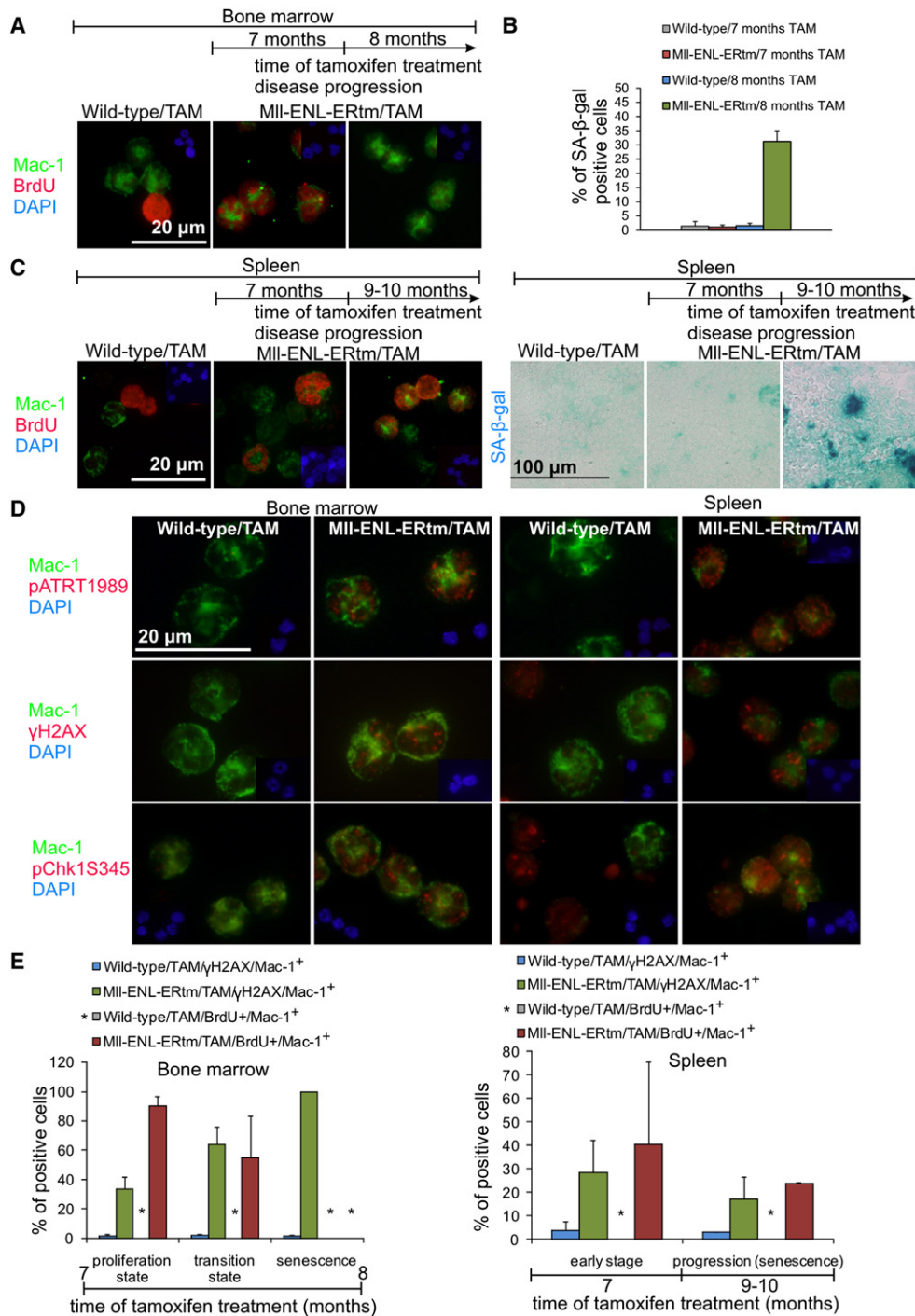


Figure 3. Tissue Specificity of Association between Proliferation Rate, Senescence, and DDR Activation in Mac-1⁺ Cells during Disease Progression

(A) BrdU-positivity (red) of Mac-1⁺ (green) cells indicates aberrant proliferation at 7 months of TAM treatment, and BrdU-negativity of Mac-1⁺ cells shows loss of proliferation by 8 months of TAM treatment in the MII-ENL-ERtm/TAM BM. Nuclei stained with DAPI (blue). Scale bar represents 20 μm.

(B) Quantification of SA-β-gal assay at 7 and 8 months of TAM treatment in the BM of MII-ENL-ERtm/TAM mice compared to wild-type controls TAM-treated for 7 months. Average percentages of SA-β-gal positive cells from two to three mice per time point ± SD.

(C) Aberrant proliferation of Mac-1⁺ cells during disease progression at 7 and 9–10 months of TAM treatment; cytospin preparations, scale bar represents 20 μm (left panel). SA-β-gal staining of spleen sections (right panel) performed at the same time points as the BrdU assay. Scale bar represents 100 μm.

(D) Activation of the ATR/Chk1/γH2AX pathway (red signals) in Mac-1⁺ (green) cells in both tissues at 7 months of TAM treatment. Nuclei stained with DAPI (blue). Scale bar represents 20 μm.

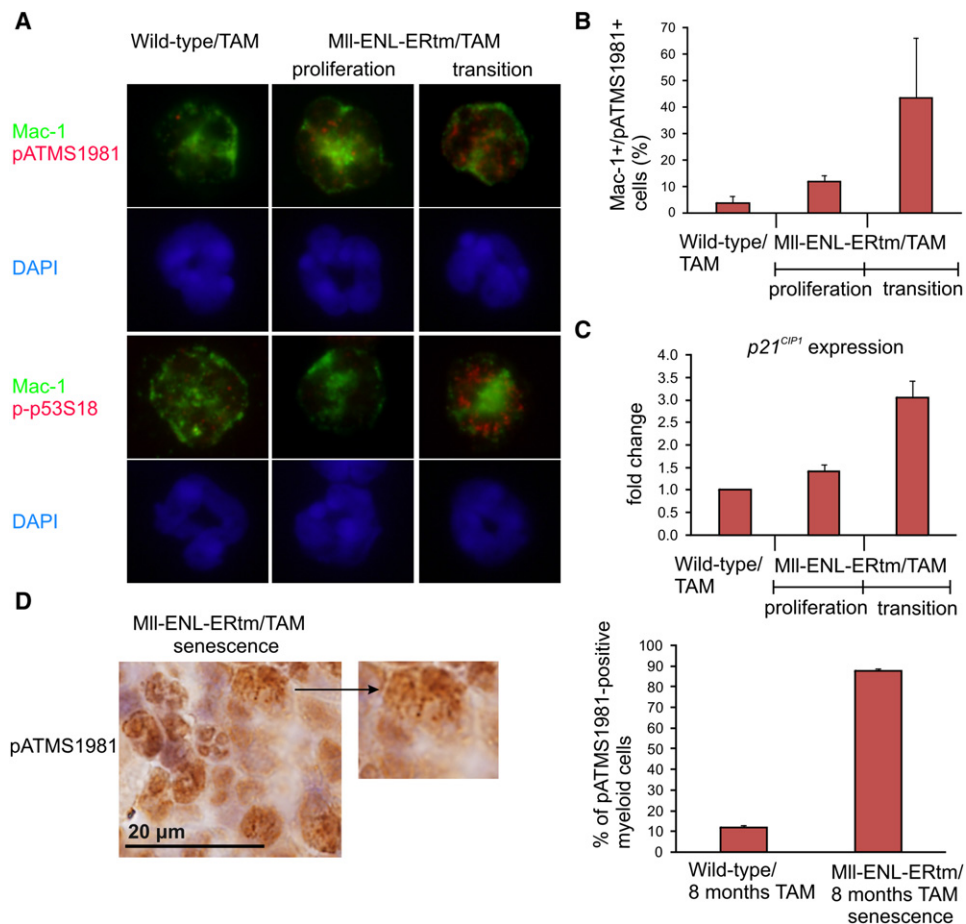


Figure 4. The ATM/p53/p21^{CIP1} Checkpoint Signaling in the Transition Cell State in the MII-ENL-ERtm/TAM BM

(A) Activation of ATM during transition from proliferation to senescence in the Mac-1⁺ cell population in the MII-ENL-ERtm/TAM BM compared to wild-type/TAM mice correlated with phosphorylated p53 (p-p53S18, bottom panel).

(B) Quantification of pATMS1981 in the proliferation and transition cell states compared to wild-type/TAM mice. Data are averages from two mice per genotype and cell state \pm SD.

(C) Expression level of p21^{CIP1} in the proliferation and transition states in the MII-ENL-ERtm/TAM BM compared to wild-type/TAM mice. Data are averages from three mice per genotype and cell state \pm SD. Each measurement performed in triplicate.

(D) Immunoperoxidase staining (left), and quantification of pATMS1981 in myeloid cells in the MII-ENL-ERtm/8 months TAM BM associated with senescence (right). pATMS1981 quantified in granulocytes in the BM of wild-type/8 months TAM mice was used as control. Scale bar represents 20 μ m. Data are averages from two mice per genotype \pm SD.

genes, and those involved in cell activation and migration (Figure 5D). The genes transiently upregulated in the BM during the high-DDR transition period, were not differentially expressed in the spleen (data not shown).

These data suggest that MLL-ENL-ERtm-induced cellular transformation is associated with altered innate and adaptive immune response, manifested as inflammation with characteristic gene expression profiles and phenotypic features that differ in the tissue environments of BM and spleen, respectively. These findings raise questions about the potential interplay and/or hierarchical order of the MLL-ENL-induced DDR activation, senescence, and the inflammatory responses.

CXCL2 and CCL3 Promote DDR Signaling and Cooperate with TNF- α to Induce Senescence in MLL-ENL-ERtm-Immortalized BM Cells

As *Cxcl2* was present in the MLL-ENL-ERtm-induced inflammatory gene set (Figure 5C), and previously implicated in RAS-evoked senescence (Acosta et al., 2008), we hypothesized that CXCL2 may contribute to the MLL-ENL-ERtm-induced DNA damage and senescence in our model. We therefore derived total BM cells from the MII-ENL-ERtm/TAM mice in the proliferation state and cultured them in the presence of GM-CSF, G-CSF, and 4-oht. Reminiscent of BM in vivo, the DDR markers pATR and γ H2AX were present in such cultured cells. Notably,

(E) Inverse correlation between proliferation and DDR in the BM over time (left). Correlation of the proliferation rate of the Mac-1⁺ spleen cells with DDR across disease stages (right). Average percentages of Mac-1⁺/BrdU⁺ and Mac-1⁺/ γ H2AX⁺ cells among total Mac-1⁺ cells, calculated from three mice per time point \pm SD. Asterisks indicate the average value = 0 for wild-type/TAM/BrdU⁺/Mac-1⁺ and MII-ENL-ERtm/TAM/BrdU⁺/Mac-1⁺ in the senescence state in the BM. See also Figure S3.

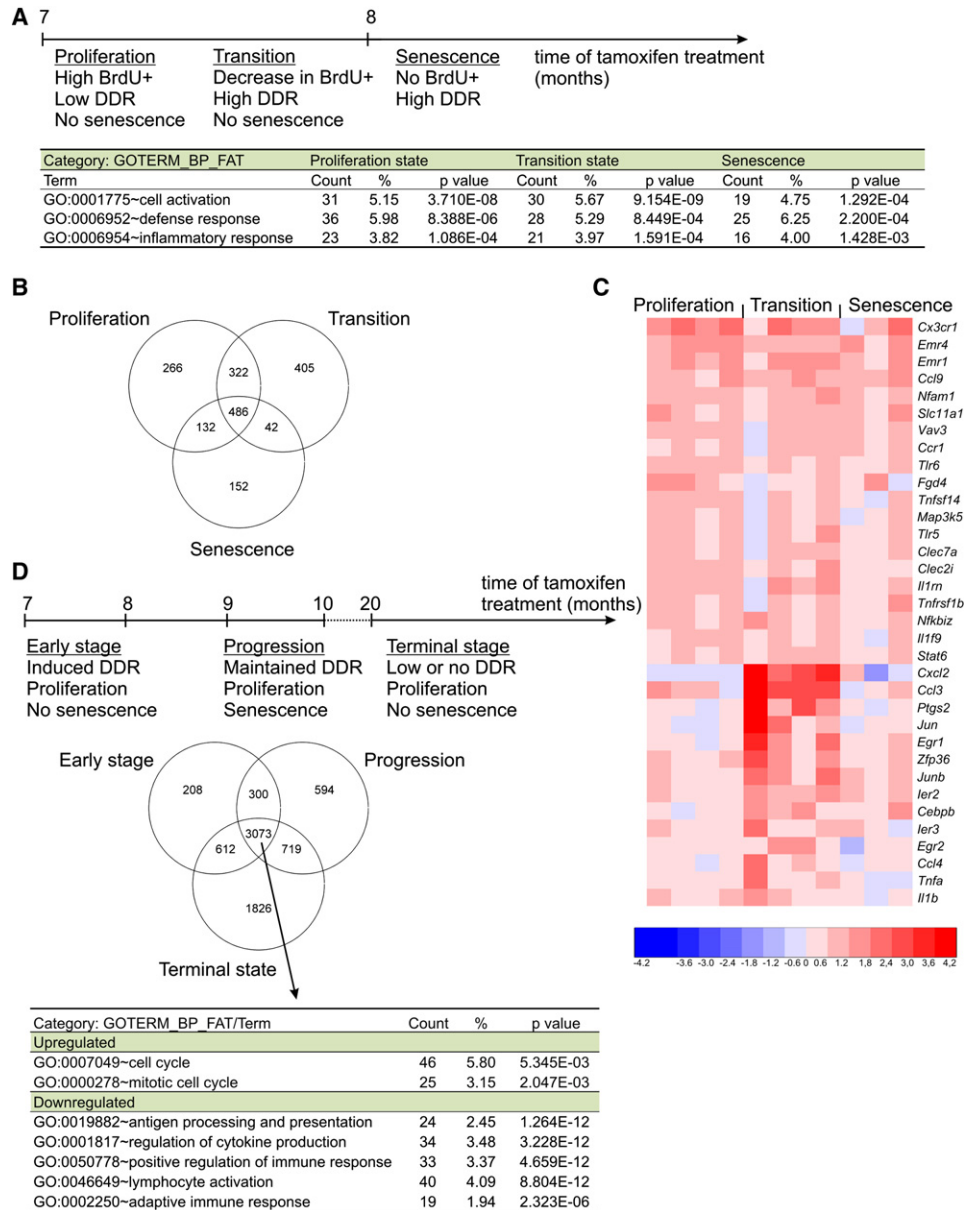


Figure 5. Gene Expression Profiling across Disease Stages and Cellular States

(A) Overrepresented GO terms in indicated cellular states in the MII-ENL-ERtm/TAM BM. GO analysis was performed on upregulated genes (5% p value cut-off, 1.5-fold change cut-off) in each cell state compared to wild-type/TAM controls.

(B) Venn diagram of differential gene expression in the BM of MII-ENL-ERtm/TAM mice across different cellular states. Differentially expressed genes (5% p value cut-off, 1.5-fold change cut-off) in each cell state were used for pairwise comparison to identify unique and shared genes. Numbers represent the up- or downregulated genes in unique sections or shared genes in each intersection.

(C) Heatmap representation of differential expression of selected genes across cell states in the MII-ENL-ERtm/TAM BM. Rows represent individual genes and columns represent individual mice. Values are indicated as log₂ ratios.

(D) Venn diagram of differential gene expression in the spleen of MII-ENL-ERtm/TAM mice across disease stages. Overrepresented GO terms in upregulated and downregulated gene sets shared between the three disease stages. The same approach and selection criteria were used as for the BM.

pATR declined upon 4-oh withdrawal indicating that ATR phosphorylation depends on continuous activity of MLL-ENL-ERtm (Figure S4A). Next, we exposed this BM culture to CXCL2, CCL3, TNF- α , and IL-1 β (each alone or in various combinations) that were part of the inflammatory expression profile during the transition period to senescence. Cells were grown for 4 days

under these conditions and assayed for γ H2AX at day 2 and SA- β -gal at day 4. The highest level of γ H2AX was observed in cultures exposed individually to chemokines CXCL2 or CCL3. Addition of TNF- α or IL-1 β alone did not significantly enhance γ H2AX (Figure 6A, left). The highest level of senescence was induced in the presence of CXCL2/TNF- α /IL-1 β ,

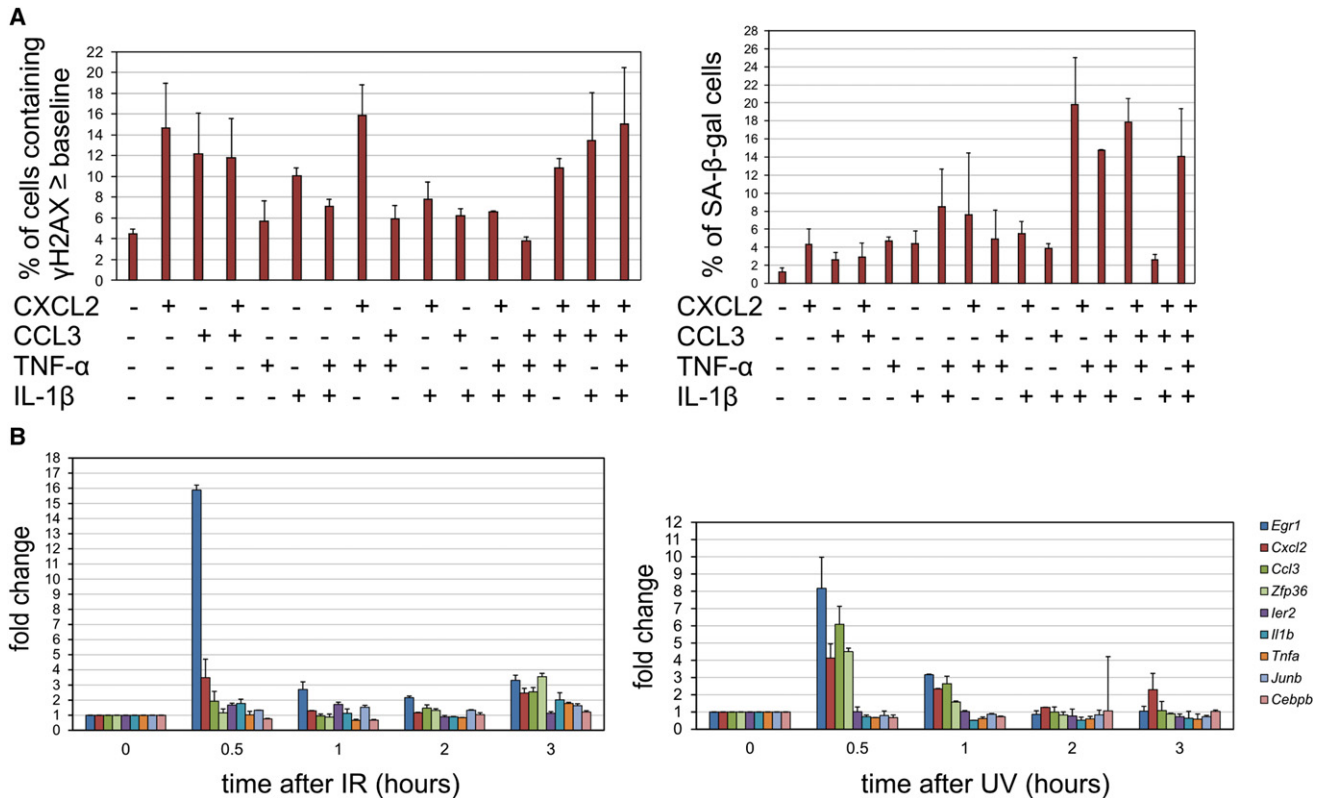


Figure 6. Cooperation of DDR and Inflammation in MLL-ENL-ERtm-Induced Senescence

(A) Effects of selected inflammatory factors on DDR in a MII-ENL-ERtm BM cell line assessed by γ H2AX staining at 48 hr of treatment. The highest level of γ H2AX in individual cells in untreated control culture (10–20 foci/nuclei) was estimated, and the relative number of these cells was counted. This level was used as a baseline threshold, and the relative number of cells containing γ H2AX foci on the baseline level or above (≥ 20 –30 foci/nuclei or an intense homogenous signal pattern) was estimated in each culture condition. Data are averages from two experiments \pm SD (left). The effect of selected inflammatory factors on senescence induction in a MII-ENL-ERtm BM cell line. The graph shows the percentage of SA- β -gal positive cells relative to total number of cells calculated in each tested conditions at day 4. Data are averages from two experiments \pm SD (right).

(B) Time course expression of selected genes from the inflammatory signature after IR in a MII-ENL-ERtm BM cell line. Data are averages from two experiments \pm SD (left). Time course of expression of selected genes from the defined inflammatory signature after UV in a MII-ENL-ERtm BM cell line. Data are averages from two experiments \pm SD (right). The same color coding was used for both graphs.

See also Figure S4.

CCL3/TNF- α /IL-1 β , CXCL2/CCL3/TNF- α , and CXCL2/CCL3/TNF- α /IL-1 β (Figure 6A, right). DDR was not increased (Figure S4B) and senescence was not induced in the control 32Dcl3 BM cells. Thus, although CXCL2 and CCL3 signaling pathways enhance the DDR in MLL-ENL-ERtm-immortalized cells, additional factors, such as TNF- α are required for MLL-ENL-ERtm-induced senescence in vitro. IL-1 β may contribute to senescence induction; however, it is ineffective on its own.

DDR Activates a Subset of the Inflammatory Signature Genes

To examine whether some genes from the defined inflammatory signature in our model might selectively respond to genotoxic insults that trigger ATR and/or ATM kinase signaling, the cultured MII-ENL-ERtm BM cells were subjected to ionizing radiation (IR) and ultraviolet light (UV) exposure, and mRNA expression was measured at 0.5, 1, 2, 3, and 6 hr after irradiation. The most up-regulated genes were *Egr1*, *Cxcl2*, and *Ccl3*, which rapidly responded to both IR and UV at the 0.5-hr time point. The *Zfp36*

gene was highly upregulated only in response to UV, whereas three genes, *Ier2*, *Ii1b* (at the 0.5-hr time point), and *Tnfa* (at the 3-hr time point), were upregulated only in response to IR (dominant ATM signaling). The expression levels of *Cebpb* and *Junb* did not change in response to either radiation treatment (Figure 6B). We conclude that *Cxcl2* and *Ccl3* are expressed very early upon DNA damage and may be coregulated with *Egr1*; furthermore *Cxcl2* has been recognized as a direct target of EGR-1 (Ramana et al., 2009). ATM-mediated signaling may contribute to the maintenance of expression levels of *Ier2*, *Ii1b*, and *Tnfa*.

The DDR-Mediated Senescence Barrier Is Eliminated during Leukemia Progression

Having established the interplay between DDR and inflammatory signaling as a candidate senescence-inducing barrier in the MII-ENL-ERtm mice, we argued that elimination or bypass of such antileukemia barrier by natural selection would be predictable for those animals that have developed the terminal disease.

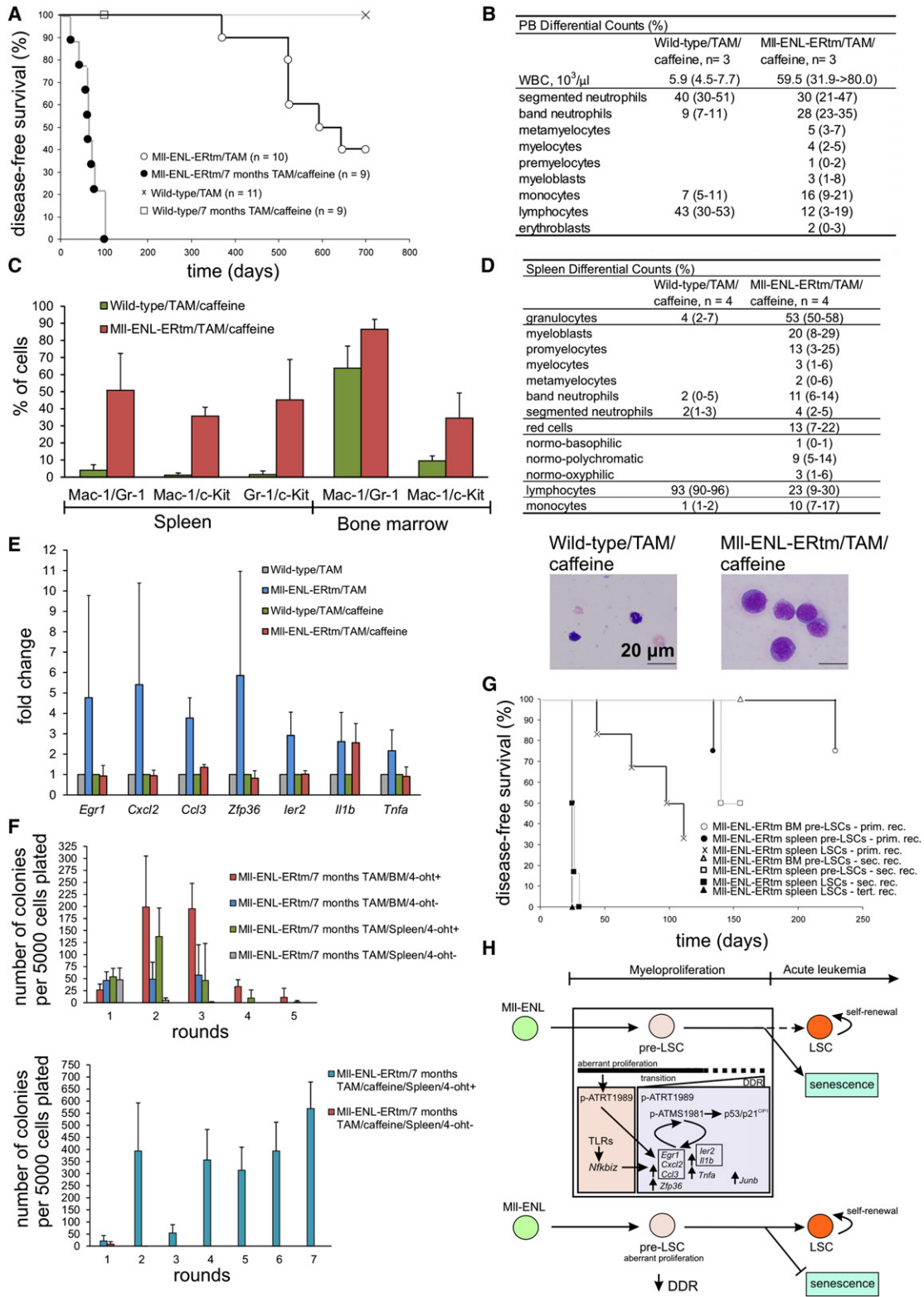


Figure 7. Caffeine Treatment Facilitates AML Development

(A) Caffeine treatment of MII-ENL-ERtm/TAM mice at the early disease stage significantly (log rank test, $p < 0.001$) reduces disease latency in vivo. (B) PB differential counts and WBC counts of caffeine-treated MII-ENL-ERtm/TAM and wild-type/TAM mice. Data are averages from three mice (data range). (C) FACS analysis shows an increase in c-Kit⁺/Mac-1⁺/Gr-1⁺ cells in the BM and spleen of caffeine-treated MII-ENL-ERtm/TAM mice compared to the early disease stage (see Figures 1C and 1E). Data are average percentages counted from three mice \pm SD.

Analyses of DDR signaling and senescence in the spleen of such mice showed sustained pATR, however, the number of γ H2AX-positive cells was decreased compared to earlier disease stages. Notably, features of senescence were either completely absent or only residual (Figure S5A). These results suggest that development to a more advanced stage of MLL-ENL-ERtm-driven leukemia is associated with reduced DDR signaling itself (lower γ H2AX) and/or elimination/bypass of the downstream impact of DDR signaling, below the threshold required for senescence. Such a scenario is also consistent with an overall increase in the Mac-1⁺/c-Kit⁺ cell population in the spleen throughout disease progression (Figure 1E) indicating that this population gains selective advantage of limitless growth.

Barrier Inhibition Accelerates Cellular Transformation toward a More Immature Cell State

To test our concept of DDR as a driving force of cytokine expression and senescence induction that may delay or prevent the MLL-ENL-ERtm-mediated transformation in vivo, we assessed whether chemical silencing of DDR could impact the kinetics of disease progression in our model. To inhibit DDR in vivo, the MII-ENL-ERtm/TAM mice at the early disease stage and wild-type/TAM controls (7 months of TAM treatment) were subjected to continuous treatment by caffeine, a commonly used inhibitor of both ATM and ATR kinases. Striking acceleration of the disease was observed in the MII-ENL-ERtm mice that showed signs of disease with a mean survival of 62 ± 23 days of caffeine treatment (Figure 7A). PB differential counts showed high numbers of band neutrophils and monocytes (Figure 7B). Notably, FACS profiling revealed increased c-Kit⁺/Mac-1⁺/Gr-1⁺ cell populations in the spleen and the BM (Figure 7C) compared to the early stage phenotype (Figures 1C and 1E). Differential counts showed a marked shift to immature myeloid elements in the spleen such as promyelocytes and myeloblasts (Figure 7D), and severe hepato-splenomegaly was apparent due to invasion of leukemia cells into tissues (Figure S5B). DDR markers were decreased in Mac-1⁺ cells both in the BM and spleen confirming the inhibition of ATR/ATM activity, and senescence

was not detected in either BM or spleen. The immunofluorescence data on tissue sections were corroborated by a sensitive immunoperoxidase staining that showed only weak to undetectable DDR markers in tissues from caffeine-treated mice, in contrast to variable and often strong nuclear focal staining in caffeine-free MII-ENL-ERtm/TAM mice (Figure S5C and data not shown).

Given that some of the inflammatory signature genes upregulated in the high-DDR MII-ENL-ERtm/TAM BM (validated with quantitative RT-PCR, Figure 7E) were responsive to DDR, we determined the expression level of these inflammatory genes (*Egr1*, *Cxcl2*, *Ccl3*, *Zfp36*, *Ier2*, *I11b*, and *Tnfa*) in the BM of the caffeine-treated MII-ENL-ERtm/TAM mice in vivo. Under such conditions, only *I11b* became upregulated (compared to wild-type/TAM/caffeine mice) whereas all other genes evaluated were expressed at the basal level despite the active MLL-ENL oncogene (Figure 7E).

We conclude that caffeine treatment is sufficient to overcome the barrier to MLL-ENL-ERtm-induced malignancy, leading to accelerated transition of committed progenitors to immature cell states during leukemia development. Caffeine treatment also prevents activation and/or leads to reversion of a large subset of the transient inflammatory gene signature, consistent with our present data that these genes are regulated in response to DDR induction.

Caffeine Treatment Promotes Acquisition of Self-Renewal Capacity and Enables Development of LSCs

We next analyzed the impact of the dual ATM/ATR inhibitor caffeine on self-renewal potential of MII-ENL-ERtm myeloid progenitors. BM and spleen cells isolated from MII-ENL-ERtm/TAM myeloproliferative mice (early stage, 7 months TAM) and spleen cells from caffeine-treated MII-ENL-ERtm/TAM AML mice were tested for their colony formation and serial replating ability in methylcellulose culture with or without 4-oht. Early stage MII-ENL-ERtm BM and spleen myeloid progenitors exhausted their ability to form colonies during the fifth round of replating in the presence of 4-oht. In contrast, MII-ENL-ERtm

(D) Differential counts from the spleen of caffeine-treated MII-ENL-ERtm/TAM show a marked shift to immature cell types compared to caffeine-treated wild-type/TAM mice. Data are averages from four mice (data range). Representative spleen smear from the caffeine-treated MII-ENL-ERtm/TAM mouse shows the morphology of promyelocytes and myeloblasts (bottom). Scale bar represents 20 μ m.

(E) Quantitative RT-PCR analysis of inflammatory gene expression in the BM of caffeine-treated MII-ENL-ERtm/TAM mice compared to caffeine-treated wild-type/TAM controls. The expression level of tested genes measured by quantitative RT-PCR in the MII-ENL-ERtm/TAM BM (transition state) compared to time-matched wild-type/TAM mice is also indicated. The results are fold changes between average expression levels measured in two to three mice per genotype \pm SD. Each measurement was performed in triplicate.

(F) Quantification of colony formation of BM and spleen cells harvested from MII-ENL-ERtm mice of indicated disease stages and treatment-conditions over five and seven rounds of replating, respectively. Data are averages from four experiments (cells derived from individual mice) \pm SD. Each experiment performed in triplicate.

(G) The MII-ENL-ERtm spleen LSC-enriched cells initiate a rapid onset of leukemia in serial transplantations (log rank tests, primary versus secondary transplants $p = 0.001$, primary versus tertiary transplants $p = 0.003$). The in vivo leukemogenic potential of the MII-ENL-ERtm spleen LSCs is significantly higher compared to MII-ENL-ERtm BM pre-LSCs (log rank, $p = 0.025$) and spleen pre-LSCs (log rank, $p = 0.025$) in secondary recipients. Prim. rec., primary recipients; sec. rec., secondary recipients; tert. rec., tertiary recipients.

(H) Model summarizing the mechanistic basis of the barrier that delays MLL-ENL-induced acute leukemia development. Top scheme: MLL-ENL initiates aberrant proliferation of myeloid cells leading to development of a pre-LSC state manifested as a myeloproliferative disorder. Cell intrinsic (ATR) and extrinsic (TLRs) signaling pathways activate a complex fail-safe program consisting of antiproliferative and inflammatory signals. Inflammatory factors fine-tune the DDR signaling toward activation of p53 that modulates the fate of pre-LSCs. A critical cell-fate decision occurs between senescence and acquisition of LSC properties such as self-renewal, a prerequisite of development to a more transformed cell state. Bottom scheme: inhibition of DDR prevents senescence and accelerates progression to AML. For detailed explanation see Discussion. Lines (arrow, activation; blunted, inhibition) represent regulatory impact. Pink square, proliferation state; violet square, transition state. Upregulated expression of inflammatory regulators is highlighted by arrows.

See also Figure S5 and Tables S1 and S2.

AML cells showed enhanced cloning efficiency and continued to form numerous colonies through all seven rounds of replating evaluated. Reversion of MLL-ENL-ERtm activity by 4-oh withdrawal both in early stage and AML cells led to formation of only mature colony types in the first and second rounds of replating (Figure 7F). We therefore identify the early stage MII-ENL-ERtm progenitors as a pre-LSC population with limited proliferation and self-renewal capacity, whereas AML cells derived from the caffeine-treated MII-ENL-ERtm mice represent a LSC-enriched population with acquired unlimited self-renewal potential.

To further assess the leukemia-initiating potential of MII-ENL-ERtm pre-LSCs and LSCs, we performed serial transplantations into TAM-treated SCID recipients. Consistent with the results from the in vitro replating assay, the MII-ENL-ERtm BM pre-LSCs induced myelomonocytic proliferation with a long latency (229 days) in one of four primary recipients and all secondary recipients remained disease-free until 165 days after transplantation. The MII-ENL-ERtm spleen pre-LSCs induced leukemia in one of four primary transplanted mice with a latency of 134 days, and in one secondary transplant with a similar latency (140 days, $n = 2$). Importantly, MII-ENL-ERtm LSC-enriched spleen cells induced leukemia with a short latency (mean: 81 ± 30 days) in four of six primary recipient mice, and in both secondary and tertiary transplants with a complete penetrance in 26 ± 2 days and 25 ± 0 days after transplantation, respectively (Figure 7G). Importantly, spleen LSC-initiated AMLs exhibited a more severe phenotype, higher numbers of myeloblasts in the analyzed tissues and higher frequency of c-Kit⁺ cells in the spleen compared with pre-LSC-induced AML in the primary transplantations (Table S1). In addition, the degree of phenotypic maturity negatively correlated with the level of DDR activation in the primary transplanted animals. We detected high level of γ H2AX in the majority of spleen cells in mice with a pre-LSC-induced myelomonocytic proliferation and leukemia. In contrast, the majority of the LSC-induced AML spleen cells were negative or weakly positive for γ H2AX. Thus, the high self-renewal activity correlates with perturbation of DDR signaling in the spleen of primary recipients (Figure S5D). Together, these results suggest that inhibition of DDR enables MII-ENL-ERtm pre-LSCs to gain self-renewal property and establish a LSC population with a long-term ability to propagate leukemia in mice.

Relevance of the DDR Pathway to Human MLL-Rearranged Leukemia

Based on the results obtained with the mouse model, two predictions could be made for MLL-rearranged human leukemia at the clinically manifest, malignant stage: 1), the upstream DDR signaling could be constitutively activated, reflecting the continuous stress caused by the MLL fusion oncogene; and 2), downstream DDR signaling and/or effector pathways would likely be disabled during the progression to advanced leukemia. To test these predictions, we analyzed BM biopsies from three patients with confirmed MLL-rearranged AML (obtained at the time of diagnosis, Table S2) and from five healthy BM donors. Paraffin sections were stained for pATR, pATM, γ H2AX, and p21^{CIP1} by immunohistochemistry. Interestingly, the majority of MLL BM cells showed strong positivity for pATM and pATR in most leukemia cells, in contrast to the largely negative staining in the normal control samples. These findings indicate that activation

of the DDR pathway does occur also during human MLL leukemogenesis, thereby supporting the relevance of our mouse model. Although the upstream signaling kinases ATM and ATR were still activated in leukemia blasts, the downstream effector events, documented here by attenuated γ H2AX and the lack of the p53 target p21^{CIP1} (Figure S5E), were consistent with the need to neutralize the DDR barrier to allow progression to full malignancy.

DISCUSSION

This study contributes to better understanding of multistep tumorigenesis and the basis for long latency of cancer development in vivo. Our data provide insights into the mechanism of transformation by *Mll* fusion oncogenes with emphasis on cellular antitumor barriers to emergence of a LSC population in a mouse model in vivo.

Using our MII-ENL-ERtm mouse model, we show that MLL-ENL triggers myeloproliferation with a potential to transform to acute leukemia. Although the aberrantly proliferating myeloid cells display differentiated morphology, a subpopulation of cells coexpressing both lineage (Mac-1) and stem cell (c-Kit) surface markers emerges at the early stage of transformation. These findings argue for a previous suggestion that MLL fusion oncogenes can reactivate stem cell properties in a context of more differentiated progenitors (Krivtsov et al., 2006). Furthermore, we show that such aberrantly reactivated proliferation/self-renewal triggers DDR and cellular senescence, reminiscent of intrinsic antitumor barrier mechanisms suggested to operate in solid tumors (Halazonetis et al., 2008). Our model also allows to study the interplay of DDR and inflammatory antitumor barriers (Campisi and d'Adda di Fagagna, 2007; Bartek et al., 2008) in response to MLL-ENL in a disease stage-specific manner and natural settings in vivo. In addition, we found tissue-dependent properties of the leukemogenesis barrier mechanisms in BM versus spleen, indicating that such fail-safe mechanisms are influenced by factors provided by the local tissue microenvironment.

Our results implicate the DDR checkpoint machinery as a crucial fail-safe mechanism that guards against progression of MLL-ENL-immortalized myeloid cells into AML. In the early, proliferative phase of the disease, we found the ATR-Chk1 kinase module as the activated upstream signaling cascade (monitored by three markers: pATR1989, pATRS428, and pChk1S345), consistent with hyperproliferation and ensuing replication-associated stress. This was evident in both spleen and BM; however, the latter tissue showed a greater extent of hyperproliferation and also activation of ATM, the kinase that responds to DNA DSBs (Kastan and Bartek, 2004) and is activated in early lesions among diverse human solid tumors (Halazonetis et al., 2008). The more prominent overall DDR activation, including the active ATM-p53-p21^{CIP1} pathway, correlated with more robust senescence phenotype at the later stages of the MLL-ENL-induced disease in the BM, compared to milder DDR response and only moderate senescence in the spleen. Thus, it appears that the exclusive ATR signaling as seen in the spleen can result in a balanced state of concomitant partial proliferation and limited degree of senescence, whereas the combined ATR/ATM-mediated robust DDR can lead to

pronounced proliferation arrest and senescence phenotype in the BM. Notably, the weaker DDR and senescence in the spleen apparently provides less protection against leukemia, because the features of terminal malignancy, if developed, were primarily manifested in the spleen.

The observed gradual increase in DDR activation associated with enhanced activation of the ATM kinase as the MLL-ENL-ERtm BM cells transit from proliferation to senescence correlated with a transcription response involving immediate early response genes (*Egr1*, *Ier2*, *Junb*, *Zfp36*) and inflammatory factor genes (*Cxcl2*, *Ccl3*, *Il1b*, *Tnfa*). We propose that ATM-mediated signaling reflects a higher, suprathreshold level of DNA damage in aberrantly proliferating BM cells, and plays a critical role in the amplification and maintenance of the DDR signaling with impact on transcription of a set of inflammatory genes. This interpretation is consistent with our result that *Egr1*, *Cxcl2*, and *Ccl3* are induced rapidly upon DNA-damaging treatments. In turn, both CXCL2- and CCL3-mediated signaling enhances DDR in cultured MLL-ENL-ERtm-immortalized cells, and we suggest that these factors might play the same role in vivo. Consistently with recent studies implicating the feedback loop signals from DDR to cytokine and cytokine receptor genes (Bartek et al., 2008), our data indicate that ATM-mediated DDR may act in a self-autonomous regulatory loop with CXCL2 and CCL3 to boost the p53/p21^{CIP1} checkpoint response and impose cell cycle arrest in damaged cells. Indeed, *Egr1*, *Cxcl2*, and *Ccl3* are induced promptly in response to DNA damage in MLL-ENL-ERtm-immortalized cells, at a time preceding p53 activation suggesting a possible coregulation of these genes in a p53-independent, DDR-dependent manner. This is consistent with previous reports that EGR-1 is required for p53-mediated apoptosis under stress conditions and in replicative senescence, and activates inflammatory cytokines (Krones-Herzig et al., 2003; Yan et al., 2000). We propose that EGR-1 might be a point of convergence between DDR and activation of chemokines *Cxcl2* and *Ccl3* (see model Figure 7H).

Our results document that in vivo treatment with caffeine, a dual ATM/ATR inhibitor prevented induction of the MLL-ENL-induced senescence in premalignant state and promoted acquisition of self-renewal capacity, establishment of LSCs and development of aggressive AML with a short latency. This is consistent with a recent report that p53 deficiency promotes transformation of committed myeloid progenitors into LSCs, by allowing acquisition of self-renewal (Zhao et al., 2010). Reduced expression of DDR markers in the tissues of caffeine-treated mice suggests that caffeine-mediated inhibition of ATM/ATR-signaling and prevention of p53 activation might be the decisive event that allows the shift to a malignant phenotype. In other words, DDR emerges as a signaling pathway that modulates the balance between senescence and acquisition of stem cell properties in immortalized pre-LSCs in the context of the MLL-ENL-ERtm-driven oncogenesis in vivo. Although we cannot exclude that some additional caffeine-targeted mechanism(s) might be involved in leukemia development, the natural selection process in our mouse model leading to AML in association with attenuation or loss of downstream DDR events supports our conclusion that inhibition of ATM/ATR-signaling plays a major role in caffeine-mediated acceleration of leukemogenesis.

Our data also point to a crucial role of the local tissue microenvironment in modulation of cell-fate choices in MLL-ENL-ERtm pre-LSCs. Inflammatory factors and their feedback loop with DDR help to fine tune such a choice toward senescence (Figure 7H). Our study provides a valuable link between inflammation and the kinetics of LSC development. In this context, it is noteworthy, that p53 loss apparently did not accelerate leukemogenesis when *MLL-ENL* was expressed from a retroviral promoter (Zuber et al., 2009). This difference could be attributable to high level of the oncogene that might override cellular checkpoints and increase the malignant potential regardless of p53 status.

We also speculate that upregulation of crucial homeostatic regulators such as *Egr1*, *Junb*, and *Zfp36* could potentially add an additional layer of regulation to the complexity of activated fail-safe mechanisms against leukemic transformation by MLL-ENL. Interestingly, EGR-1 regulates the cell cycle machinery in HSC to maintain quiescence, thereby preventing self-renewal and migration (Min et al., 2008). JUNB limits HSC proliferation and counteracts LSC properties (Santaguida et al., 2009; Steidl et al., 2006). In the hematopoietic system, *Zfp36* is upregulated during commitment from HSC to MPP, and thus correlates negatively with self-renewal, while promoting differentiation (Forsberg et al., 2010). Considered with our present data, we hypothesize that these transcription regulators might play a role in balancing the acquisition of LSC properties (self-renewal and migration) in lineage-committed progenitors.

In conclusion, our study extends the emerging concept of DDR activation as an inducible barrier against activated oncogenes and tumor progression, from solid tumors to hematological malignancies (Bartkova et al., 2005; Gorgoulis et al., 2005; Wajapeyee et al., 2010; Boehrer et al., 2009) under in vivo conditions in mice. Furthermore, our present results have important implications for understanding the tumor-suppressive role of DDR and cell-microenvironment regulatory interactions that modulate the fate of pre-LSCs and multistep development of MLL. We also report activation of DDR in clinical samples of human MLL blasts, accompanied by attenuated effector pathway(s) in such fully developed leukemia. Taken together with our mouse model, these results are consistent with a potential biological role of the DDR machinery in preventing the transition of the initiating pre-LSC population into a fully transformed population with LSC properties. These findings support the notion that uncoupling of DDR signaling from downstream checkpoint responses may allow preleukemia cells to acquire the pathological capacity for self-renewal. Selection for cells that avoid the full impact of DDR signaling during leukemia development is relevant both conceptually, and with respect to clinical responses to standard-of-care genotoxic therapy.

EXPERIMENTAL PROCEDURES

Generation of the MLL-ENL-ERtm Knock-In ESC Clone

The creation of the mouse *MLL-ENL-ERtm* knock-in allele by gene targeting in mouse ESCs, Southern blot analyses, and generation of mice were performed as described in Supplemental Experimental Procedures.

Tissue Culture

Mouse ESCs were cultured as described in Supplemental Experimental Procedures. MLL-ENL-ERtm BM cells were cultured in RPMI (high glucose,

glutamax, sodium pyruvate) supplemented with 10% FBS (GIBCO), 10 ng/ml GM-CSF (Biosource), 10 ng/ml G-CSF (Biosource), and 100 nM 4-ohT (Sigma). 32Dcl3 mouse BM cell line was cultured in RPMI (high glucose, glutamax, sodium pyruvate) supplemented with 10% FBS (GIBCO) and 10 ng/ml IL-3 (Biosource). Recombinant mouse CXCL2, CCL3, TNF- α , and IL-1 β were purchased from R&D Systems and used at a final concentration of 50 ng/ml. Cells were irradiated with a single dose of 4 Gy IR or 20 Jm⁻² UV.

Mice

All mice were housed and treated at the Animal Research Facility at Faculty of Medicine and Dentistry, Palacky University in Olomouc. Animal experiments were approved by the institutional care and use committees for animal research. Mice were treated with TAM (Sigma) in concentration of 300 mg/kg chow. Mice were treated with caffeine (Sigma) in concentration of 0.4 mg/ml drinking water (Bartkova et al., 2006; Lu et al., 2008). BrdU (Sigma) was dissolved in sterile water and injected intraperitoneally in a dose of 100 mg/kg. Mice were analyzed 2 hr after injection.

Transplantation Assay

A total of 1–2 × 10⁷ spleen cells were injected intravenously into SCID recipients treated with TAM in concentration of 100 mg/kg chow. Mice were monitored for disease development. Kaplan-Meier statistical analysis with log rank test was used to compare survival curves.

Methylcellulose Culture

Colony forming and replating assays were performed as described in Supplemental Experimental Procedures.

FACS Analysis

Labeling of cells for FACS was performed on ice in phosphate-buffered saline (PBS) supplemented with 0.5% bovine serum albumin (BSA) (Sigma) using conjugated antibodies purchased from BD Pharmingen. Details of the antibodies used can be found in Supplemental Experimental Procedures.

RT-PCR

RT-PCR was performed with the Stratagene Brilliant II SYBR Master Mix. Each sample was analyzed in triplicate using cDNA corresponding to 10 ng of total RNA reverse transcribed with Superscript III (Invitrogen) according to the manufacturer's recommendations.

Quantitative RT-PCR

Total tissue RNA was isolated using the RNeasy kit (QIAGEN). Reverse transcription was performed using the First Strand cDNA Transcriptor Synthesis kit (Roche). RT-PCR detection was performed using the Universal ProbeLibrary probe/primers sets in triplicate for each sample and reactions were run on the LightCycler 480 system (Roche). *Ywhaz* and *Gapdh* were used as a reference for all reactions. Relative expression was calculated by the 2DDCT method.

Gene Expression Microarray and Bioinformatics Analyses

Total tissue RNA was isolated as described above. RNA was amplified, labeled, and hybridized to Mouse 430A 2.0 genomic arrays (Affymetrix). Differential expression analysis and normalization of chip data was performed in the R statistical environment (The R Project for Statistical Computing, version 2.9.2) using the Limma and Affy packages from Bioconductor project (<http://www.bioconductor.org>). Differentially expressed genes were identified using ImFit function (moderated t statistics) and Benjamini-Hochberg corrected ($p < 0.05$). GO analysis were conducted using Database for Annotation, Visualization and Integrated Discovery (DAVID) (<http://david.abcc.ncifcrf.gov/>). For GO and heatmap, only genes with at least 1.5-fold difference between averages of the MLI-ENL-ERTm and the corresponding wild-type sample group were selected.

Immunofluorescence Analysis

Cells were fixed on glass slides in 3% paraformaldehyde at room temperature (RT) for 15 min, permeabilized in methanol at -20°C for 10 min and air-dried, incubated in 1% or 10% BSA (optional) in PBS for 1 hr at RT, followed by primary antibodies at 4°C overnight. Alexa Fluor-conjugated secondary anti-

bodies were incubated at RT for 1 hr. Antibodies used are listed in Supplemental Experimental Procedures. For Mac-1/BrdU double staining, cells were first stained for Mac-1 as described above, fixed again in 3% paraformaldehyde and then DNA was denatured in 2 M HCl for 30 min at 37°C. After neutralization in PBS, samples were blocked with 1% BSA in PBS and incubated with the anti-BrdU antibody conjugated with Alexa594 dye (Invitrogen) for 1 hr at RT. Images were acquired using an Olympus BX51 inverted microscope equipped a ColorViewIII digital CCD camera. Validation of antibodies to pATRS428 and pATRT1989 is shown in Figure S3B.

Immunohistochemistry

Formalin-fixed tissues were paraffin embedded, sectioned at 3–5 μ m, and H&E stained. Immunohistochemical analyses were performed as described in detail in the Supplemental Experimental Procedures.

Senescence Assay

Cytospin preparations of BM cells and cryostat spleen sections were used. SA- β -gal was detected by the Senescence detection kit (Calbiochem) according to manufacturer's instructions.

Human Samples

Human BM samples were obtained from the Department of Clinical and Molecular Pathology, University Hospital Olomouc (UHOL), Olomouc, Czech Republic. Diagnostic data related to patient samples were provided by the Department of Hemato-Oncology, UHOL. The original examinations were obtained with the approval of the IRB committee of the UHOL and according to the Declaration of Helsinki. Additional information on patient samples is available in Table S2.

ACCESSION NUMBERS

Microarray data have been deposited at the Gene Expression Omnibus (GSE35038).

SUPPLEMENTAL INFORMATION

Supplemental Information includes five figures, two tables, and Supplemental Experimental Procedures and can be found with this article online at doi:10.1016/j.ccr.2012.01.021.

ACKNOWLEDGMENTS

We thank Dalibor Dolezal and the Animal facility, Faculty of Medicine and Dentistry, Palacky University, Olomouc (FMD-PUO) for assistance; the transgenic facility of the University Erlangen, Erlangen, Germany for ESC injection and animal husbandry; Jan Honetschlager (Institute of Molecular Genetics, Prague) for animal husbandry; Lucie Piterkova (FMD-PUO) for assistance with mouse analyses; the members of the Department of Histology and Embryology, FMD-PUO for some of the immunohistochemical staining; the members of the Department of Hemato-Oncology, UHOL, Olomouc for blood and tissue differential counts; and Jiri Zavdil and the NYU Cancer Institute Genomics Facility, New York, USA for performing and analyzing some of the gene expression arrays. Grant support from: the Czech Ministry of Education (NPV2B06077, MSM6198959205) to V.D., (MSM6198959216) to J.B., the Czech Grant Agency (GA301/01/0489) to V.D., the German research council (DFG grant SL277-1) to R.S., the Grant Agency of the Czech Academy of Sciences (IAA501370902), the Czech Ministry of Health (NS10282-3/2009), the Danish National Research Foundation, the Danish Cancer Society, the European Commission (projects Infla-Care, Biomedreg: CZ.1.05/2.1.00/01.0030, DDRresponse) to J.B.

Received: October 26, 2010

Revised: June 10, 2011

Accepted: January 25, 2012

Published: April 16, 2012

REFERENCES

- Acosta, J.C., O'Loughlen, A., Banito, A., Guijarro, M.V., Augert, A., Raguz, S., Fumagalli, M., Da Costa, M., Brown, C., Popov, N., et al. (2008). Chemokine signaling via the CXCR2 receptor reinforces senescence. *Cell* 133, 1006–1018.
- Bartkova, J., Horejsi, Z., Koed, K., Krämer, A., Tort, F., Zieger, K., Guldborg, P., Sehested, M., Nesland, J.M., Lukas, C., et al. (2005). DNA damage response as a candidate anti-cancer barrier in early human tumorigenesis. *Nature* 434, 864–870.
- Bartkova, J., Rezaei, N., Liontos, M., Karakaidos, P., Kletsas, D., Issaeva, N., Vassiliou, L.V., Kolettas, E., Niforou, K., Zoumpourlis, V.C., et al. (2006). Oncogene-induced senescence is part of the tumorigenesis barrier imposed by DNA damage checkpoints. *Nature* 444, 633–637.
- Bartek, J., Hodny, Z., and Lukas, J. (2008). Cytokine loops driving senescence. *Nat. Cell Biol.* 10, 887–889.
- Boehrer, S., Adès, L., Tajeddine, N., Hofmann, W.K., Kriener, S., Bug, G., Ottmann, O.G., Ruthardt, M., Galluzzi, L., Fouassier, C., et al. (2009). Suppression of the DNA damage response in acute myeloid leukemia versus myelodysplastic syndrome. *Oncogene* 28, 2205–2218.
- Campisi, J., and d'Adda di Fagagna, F. (2007). Cellular senescence: when bad things happen to good cells. *Nat. Rev. Mol. Cell Biol.* 8, 729–740.
- Chen, W., Kumar, A.R., Hudson, W.A., Li, Q., Wu, B., Staggs, R.A., Lund, E.A., Sam, T.N., and Kersey, J.H. (2008). Malignant transformation initiated by MLL-AF9: gene dosage and critical target cells. *Cancer Cell* 13, 432–440.
- Cozzio, A., Passegué, E., Ayton, P.M., Karsunky, H., Cleary, M.L., and Weissman, I.L. (2003). Similar MLL-associated leukemias arising from self-renewing stem cells and short-lived myeloid progenitors. *Genes Dev.* 17, 3029–3035.
- Di Micco, R., Fumagalli, M., Cicalese, A., Piccinin, S., Gasparini, P., Luise, C., Schurra, C., Garre, M., Nuciforo, P.G., Bensimon, A., et al. (2006). Oncogene-induced senescence is a DNA damage response triggered by DNA hyper-replication. *Nature* 444, 638–642.
- Dimri, G.P., Lee, X., Basile, G., Acosta, M., Scott, G., Roskelley, C., Medrano, E.E., Linskens, M., Rubelj, I., Pereira-Smith, O., et al. (1995). A biomarker that identifies senescent human cells in culture and in aging skin in vivo. *Proc. Natl. Acad. Sci. USA* 92, 9363–9367.
- Dobson, C.L., Warren, A.J., Pannell, R., Forster, A., Lavenir, I., Corral, J., Smith, A.J.H., and Rabbitts, T.H. (1999). The mll-AF9 gene fusion in mice controls myeloproliferation and specifies acute myeloid leukaemogenesis. *EMBO J.* 18, 3564–3574.
- Forsberg, E.C., Passegué, E., Prohaska, S.S., Wagers, A.J., Koeva, M., Stuart, J.M., and Weissman, I.L. (2010). Molecular signatures of quiescent, mobilized and leukemia-initiating hematopoietic stem cells. *PLoS ONE* 5, e8785.
- Gorgoulis, V.G., Vassiliou, L.V., Karakaidos, P., Zacharatos, P., Kotsinas, A., Liloglou, T., Veneri, M., Dittullo, R.A., Jr., Kastrinakis, N.G., Levy, B., et al. (2005). Activation of the DNA damage checkpoint and genomic instability in human precancerous lesions. *Nature* 434, 907–913.
- Halazonetis, T.D., Gorgoulis, V.G., and Bartek, J. (2008). An oncogene-induced DNA damage model for cancer development. *Science* 319, 1352–1355.
- Kastan, M.B., and Bartek, J. (2004). Cell-cycle checkpoints and cancer. *Nature* 432, 316–323.
- Krivtsov, A.V., Twomey, D., Feng, Z., Stubbs, M.C., Wang, Y., Faber, J., Levine, J.E., Wang, J., Hahn, W.C., Gilliland, D.G., et al. (2006). Transformation from committed progenitor to leukaemia stem cell initiated by MLL-AF9. *Nature* 442, 818–822.
- Krones-Herzig, A., Adamson, E., and Mercola, D. (2003). Early growth response 1 protein, an upstream gatekeeper of the p53 tumor suppressor, controls replicative senescence. *Proc. Natl. Acad. Sci. USA* 100, 3233–3238.
- Littlewood, T.D., Hancock, D.C., Danielian, P.S., Parker, M.G., and Evan, G.I. (1995). A modified oestrogen receptor ligand-binding domain as an improved switch for the regulation of heterologous proteins. *Nucleic Acids Res.* 23, 1686–1690.
- Liu, S., Shiotani, B., Lahiri, M., Maréchal, A., Tse, A., Leung, C.C., Glover, J.N., Yang, X.H., and Zou, L. (2011). ATR autophosphorylation as a molecular switch for checkpoint activation. *Mol. Cell* 43, 192–202.
- Lu, Y.P., Lou, Y.R., Peng, Q.Y., Xie, J.G., Nghiem, P., and Conney, A.H. (2008). Effect of caffeine on the ATR/Chk1 pathway in the epidermis of UVB-irradiated mice. *Cancer Res.* 68, 2523–2529.
- Min, I.M., Pietramaggiore, G., Kim, F.S., Passegué, E., Stevenson, K.E., and Wagers, A.J. (2008). The transcription factor EGR1 controls both the proliferation and localization of hematopoietic stem cells. *Cell Stem Cell* 2, 380–391.
- Nam, E.A., Zhao, R., Glick, G.G., Bansbach, C.E., Friedman, D.B., and Cortez, D. (2011). Thr-1989 phosphorylation is a marker of active ataxia telangiectasia-mutated and Rad3-related (ATR) kinase. *J. Biol. Chem.* 286, 28707–28714.
- Rakoff-Nahoum, S., and Medzhitov, R. (2009). Toll-like receptors and cancer. *Nat. Rev. Cancer* 9, 57–63.
- Ramana, C.V., Cheng, G.-S., Kumar, A., Kwon, H.-J., and Enelow, R.I. (2009). Role of alveolar epithelial early growth response-1 (Egr-1) in CD8+ T cell-mediated lung injury. *Mol. Immunol.* 47, 623–631.
- Rodier, F., Coppé, J.-P., Patil, C.K., Hoeijmakers, W.A.M., Muñoz, D.P., Raza, S.R., Freund, A., Campeau, E., Davalos, A.R., and Campisi, J. (2009). Persistent DNA damage signalling triggers senescence-associated inflammatory cytokine secretion. *Nat. Cell Biol.* 11, 973–979.
- Santaguida, M., Schepers, K., King, B., Sabnis, A.J., Forsberg, E.C., Attema, J.L., Braun, B.S., and Passegué, E. (2009). JunB protects against myeloid malignancies by limiting hematopoietic stem cell proliferation and differentiation without affecting self-renewal. *Cancer Cell* 15, 341–352.
- Steidl, U., Rosenbauer, F., Verhaak, R.G., Gu, X., Ebralidze, A., Otu, H.H., Klippel, S., Steidl, C., Bruns, I., Costa, D.B., et al. (2006). Essential role of Jun family transcription factors in PU.1 knockdown-induced leukemic stem cells. *Nat. Genet.* 38, 1269–1277.
- Yan, S.-F., Fujita, T., Lu, J., Okada, K., Shan Zou, Y., Mackman, N., Pinsky, D.J., and Stern, D.M. (2000). Egr-1, a master switch coordinating upregulation of divergent gene families underlying ischemic stress. *Nat. Med.* 6, 1355–1361.
- Wajapeyee, N., Wang, S.Z., Serra, R.W., Solomon, P.D., Nagarajan, A., Zhu, X., and Green, M.R. (2010). Senescence induction in human fibroblasts and hematopoietic progenitors by leukemogenic fusion proteins. *Blood* 115, 5057–5060.
- Wang, D., and Dubois, R.N. (2010). The role of COX-2 in intestinal inflammation and colorectal cancer. *Oncogene* 29, 781–788.
- Wang, J., Iwasaki, H., Krivtsov, A., Febbo, P.G., Thorne, A.R., Ernst, P., Anastasiadou, E., Kutok, J.L., Kogan, S.C., Zinkel, S.S., et al. (2005). Conditional MLL-CBP targets GMP and models therapy-related myeloproliferative disease. *EMBO J.* 24, 368–381.
- Zhao, Z., Zuber, J., Diaz-Flores, E., Lintault, L., Kogan, S.C., Shannon, K., and Lowe, S.W. (2010). p53 loss promotes acute myeloid leukemia by enabling aberrant self-renewal. *Genes Dev.* 24, 1389–1402.
- Zuber, J., Radtke, I., Pardee, T.S., Zhao, Z., Rappaport, A.R., Luo, W., McCurrach, M.E., Yang, M.M., Dolan, M.E., Kogan, S.C., et al. (2009). Mouse models of human AML accurately predict chemotherapy response. *Genes Dev.* 23, 877–889.